https://doi.org/10.5194/egusphere-2024-3838
Preprint. Discussion started: 21 February 2025

Accurate and fast prediction of radioactive pollution by Kriging coupled with Auto-Associative Models

Raphaël Périllat[1], Sylvain Girard[1], and Irène Korsakissok[2]

[1]Phimeca, Paris, France
[2]ASNR, Paris, France

Correspondence: Raphaël Périllat (perillat@phimeca.com)

Abstract. Uncertainty estimation is a key issue in nuclear crisis situations. Probabilistic methods for taking uncertainties into account in assessments are often costly in terms of the number of simulations and computation time. This is why emulation methods, which enable rapid estimation of numerical model outputs, represent a promising solution. The main limitation of emulation methods is that they can only predict scalar quantities. In a crisis context, decisions are often based on dose maps, which are mathematically represented by high-dimensional data. In this study, we use the Auto-Associative Model method to reduce the dimension of dose results, in order to then predict these reduced data by Kriging. We also compare this prediction method with others used by the French Nuclear Safety and Radiation Protection Authority (ASNR) to predict the consequences of a nuclear accident.

1 Introduction

1.1 Context

In the event of a nuclear accident, numerical simulations of atmospheric dispersion are used to predict the territories potentially impacted by radioactive releases. The French Authority for Nuclear Safety and Radiation Protection (ASNR) develops and uses atmospheric dispersion models embedded within its operational crisis platform called C3X to perform these calculations (Tombette et al., 2014). These simulations are used to infer operational indicators such as the maximum distance from the source where a dose threshold will be exceeded. The thresholds may be, for instance, regulatory protective action guide levels that could trigger protective actions such as population evacuation, sheltering, stable iodine prophylaxis or food restrictions (de l'intérieur).

Such evaluations are subject to uncertainties due to lack of information on the installation's status, meteorological forecast uncertainties, and models' approximations (Leadbetter, S.J. et al., 2020; LE et al., 2021). Prediction errors can induce two kinds of wrong decisions: either insufficient population protection zones, where a threshold exceedance occurs but was not predicted, or unnecessary actions zones where a threshold exceedance is forecast but does not come true. While the detriment to the population in the former case is obvious, leading to the use of conservative evaluations designed to avoid this situation at all costs, limiting evacuation and other restrictions where possible is also desirable, as these actions may have a high and potentially long-term economical and health cost (Nomura et al., 2013, 2016). A better quantification of uncertainties may

https://doi.org/10.5194/egusphere-2024-3838
Preprint. Discussion started: 21 February 2025

help refine the hypotheses and potentially reduce the margins of the conservative assumptions, while ensuring a sufficient population protection. In the approach applied by the ASNR's emergency center, the very first response generally relies on pre-calculated scenarios, whose data are gathered in an "Accident Type Sheet" (ATS). This database relies on calculations carried out in the preparedness phase for a number of accidental scenarios and for selected weather situations described by a few parameters (wind direction and speed, atmospheric stability, rain), assumed to be constant in time and homogeneous over the simulation domain. In a second step, ASNR uses its local scale Gaussian puff atmospheric dispersion model called pX to obtain predictions that correspond more closely to the actual accidental and meteorological situation (Korsakissok et al., 2013).

Forecasting tools must be compatible with emergency response time constraints, when the first evaluations should be provided typically within one hour after the alert. This timing includes not only the computational time required to set up and run the simulations themselves, but also the time required to gather meteorological forecasts and source term assessment, analyse the results and communicate them to decision makers. Thus, a numerical model such as the Gaussian puff model pX (), requiring typically a few minutes to run, can be used for a single, deterministic estimation. However, the computation time required to account for uncertainties by using hundreds of simulations does not fit with these operational constraints.

1.2 Emulation and dimension reduction

An emulator is a substitution model built to run much faster than the original. It is an approximation of the function linking the inputs with one of its scalar outputs, often built by interpolation from a sample of simulations.

In the framework of radiological crisis response, emulators offer multiple attractive applications:

- Enlarge the pre-calculated scenario database by including a variety of input parameters, allowing to evaluate results for a larger range of meteorological situations than those considered in the ATS;
- Replace the original model in the case of uncertainty estimation (Le et al., 2018) or sensitivity analyses (Girard et al., 2016), where several hundreds of simulations are needed to perturb the model inputs in order to obtain a large number of outputs;
- Thanks to their speed, they allow interactive exploration of the input space, with a graphical interface where it is possible to vary the model inputs to observe their influence on the output. Such a tool can be used for education and training purposes, in order to demonstrate the influence of input parameters on the outputs and to help making "reasonably conservative" evaluations of uncertain parameter values.

In the field of atmospheric dispersion modelling, emulators have been used to predict spatio-temporal averages quantities, values at a monitoring point (Le et al., 2018) (Girard et al., 2016), or maximum exceedance distances (Périllat et al., 2020). The main limitation of emulators currently used for these applications is that they can only predict scalar outputs. Fitting an emulator for each grid point of a two-dimensional map would be both both difficult to calculate and to implement, because it would not account for the spatial structure of the data. For these reasons, emulating a spatial map requires a first step of dimension reduction.

https://doi.org/10.5194/egusphere-2024-3838
Preprint. Discussion started: 21 February 2025

The most widely used dimension reduction method is Principal Component Analysis (PCA) (Jolliffe and Cadima, 2016) (Jolliffe, 2002). It consists in projecting a set of points onto a vector subspace in a least squares optimal way, in order to obtain the most faithful representation of this set of points in a reduced dimensional subspace. It has been applied in the specific domain of atmospheric dispersion, sometimes in combination with emulation (Burgin et al., 2017) (Le et al., 2018) (Mallet et al., 2018) (Swallow et al., 2017) (Lumet et al., 2025). However, being a linear approximation, PCA fails to encode sets of map that are too different from one another.

The Auto-Associative Models (AAM) is a extension of PCA that allows to capture nonlinear structures (Girard, 2000): the dataset is approximated by a differentiable manifold instead of a linear vector space. AAM has been used once to analyse a set of maps simulated with a dispersion model (Girard et al., 2020). The method allows to parameterize a dataset by only few parameters, which can be seen as coordinates.

The present paper present the first combination of AAM with emulation, applied to the prediction of dose maps in case of an accidental release of radioactive materials in the atmosphere. We present the case study in section 2, the methods in section 3 and the results in section 4. We develop and validate separately the AAM in section 4.1.1, the Kriging in section 4.1.2, and then the whole emulation method in section 4.1.3. The validation is done on an operational case for the prediction of threshold exceedance zones. We validate the performance of this coupling against other prediction methods in 4.

2 Case study

We simulated the result of a primary breach leading to a total core meltdown in one hour of a 1300 MWe Pressurized Water Reactor. This accidental scenario is one of the pre-calculated scenarios leading to the exceeding of protective action guide levels over significant distances. We used the pX Gaussian puff dispersion model with the Doury diffusion model in neutral atmospheric stability and with a meandering wind coefficient of 3. The meandering wind coefficient is a multiplicative factor applied to the diffusion model and designed to account for wind direction variations that occur during the time span of the release and are not taken into account by the meteorological inputs.

We focused here on 2D maps of thyroid inhalation equivalent dose, 24 hours after the beginning of the releases. In France, stable iodine prophylaxis is related to a dose criteria of 50 mSv to the thyroid. We used a polar mesh with smaller cells close the source, where there are strong spatial dose variations. The nodes of the mesh are distributed on 36 angles between 0 and 360° and on 61 different radii from 500 m, increasingly spaced from each other as we move away from the source, until a distance of 30 km.

Thus, the output data has a dimension of 2196. The case study is stationary: inputs are assumed to be constant in time and space. This is not generally the case for meteorological variables, but is consistent with the simple situations on which pre-calculated sheets are based. We considered six sources of uncertainty as inputs of the model, which are listed in Table 1. Two of them are related to the meteorological situation: the wind module and rainfall rate ; two uncertain parameters, the source amplitude (a multiplicative factor applied to the source term computed for the chosen accidental scenario) and release height,

https://doi.org/10.5194/egusphere-2024-3838
Preprint. Discussion started: 21 February 2025

describe the source term characteristics; and the two last parameters are used to define radionuclide deposition rates, for iodine and others.

The choice of uncertain parameters and their ranges of variation is not representative of the full range of possible situations, but is designed to cover the most frequent use cases. For instance, the source term computed for the accidental scenario comprises 224 radionuclides, each of them being associated to a release rate as a function of time. It was computed with conservative assumptions as to the quantity of radioactive materials emitted in the atmosphere; therefore, the multiplicative factor applied to these quantities is supposed to vary between 0 and 100%, as the evaluation of the installation status at the time of the accident is more likely to lead to a decrease in the source term. In addition, uncertainties in parameters such as the ratio between the release rate of different radionuclides, or model parameters such as deposition velocity and scavenging coefficient, are not taken into account in this study, as they are of lesser importance in a first approach (Girard et al., 2014).

Table 1. Input parameters and ranges of variation for the construction of emulators.

Input variable	Range of variation	Units
Wind module	[0, 10]	$m.s^{-1}$
Rain intensity	[0, 10]	$mm.h^{-1}$
Release height	[0, 100]	m
Source term amplitude	[10, 100]	%
Deposition velocity of iodine	$[1 \times 10^{-5}, 1 \times 10^{-2}]$	$m.s^{-1}$
Deposition velocity of other elements	$[5 \times 10^{-4}, 5 \times 10^{-3}]$	$m.s^{-1}$

3 Emulation method

3.1 Auto-Associative Models

"Reducing the dimension" of an ensemble embedded in a high dimensional vector space consists in building an associated ensemble, with a lower dimensional coordinate system. A rough definition of topological dimension would be "the minimum number of variables needed to represent a set" (Fukunaga and Olsen, 1971). More rigorously, we must choose the nature of the associated sets in order to have a precise definition of "coordinate system", for example the one recalled by (Milnor, 1997) for differentiable manifold.

Given a set $G \subset \mathbb{R}^m$, with a large m, we try to construct the approximate set $A \subset \mathbb{R}^m$ in bijection with the vector space $C \subset \mathbb{R}^l$, with l small (see figure 1).

https://doi.org/10.5194/egusphere-2024-3838
Preprint. Discussion started: 21 February 2025

Figure 1. Principle of dimension reduction.

The Auto-Associative Models (Girard and Iovleff, 2008) is a nonlinear method of dimension reduction. The term "linear" here means that the approximating space A would be a sub-vector space and $\chi \circ \psi$ an orthogonal projection. In contrast, in the "nonlinear" case, the approximating space A is a differentiable manifold and $\chi \circ \psi$ a composition of orthogonal projections by a nonlinear χ function.

3.2 Kriging

Kriging is a spatial interpolation method and the core of geostatistics. It was originally designed for optimizing gold mining (Chilès and Delfiner, 1999) by inferring from a few boreholes the spatial distribution of gold grades over the whole mining field. Kriging becomes an emulation method by replacing the spatial coordinates by the model inputs, and gold grade by the scalar model output.

The Kriging emulator predicts the value of the model output as a linear combination of a sample of pre-computed values, the learning sample. The weights of the linear combination depend only on the relative positions of the target and learning points in the input space. More precisely, they are uniquely determined as the solution of the minimization of the variance of the prediction error.

This variance is defined by assuming that the response surface, namely the surface spanned by the output when the inputs vary, is a realization of a square integrable random process. The random process is assumed to be second order stationary, which means that its expectation is constant, and the covariance between values at two points depends solely on their (vector) distance.

For a process with null expectation, the weights $w_1, \ldots, w_N$ are the solution of the following system

$$\forall 1 \leq i \leq N, \quad \sum_{j=1}^{N} w_j \, K(x_i, x_j) + \lambda = K(x, x_i), \tag{1}$$

$$\sum_{j=1}^{N} w_j = 1, \tag{2}$$

where $K(\cdot,\cdot)$ is the covariance kernel, $x_1, \ldots, x_N$ are the training points in the input space, λ a Lagrange multiplier and x the target point in the input space. The centered prediction at x is then given by $\hat{f}(x) = \sum_{i=1}^{N} w_j f(x_i)$, where $f(x_i)$ are the pre-computed values at the training points. The (usually non null) expectation is also estimated by a linear combination of the pre-computed values and added to the prediction. The weights for the expectation estimator verify a similar equation system as (1) with a null second member in the first line.

https://doi.org/10.5194/egusphere-2024-3838
Preprint. Discussion started: 21 February 2025

We used the R package DiceKriging (Roustant et al., 2012) which provides a choice of second order stationary covariance kernels.We used a tensor product of identical kernels, one for each input variable. We fitted the parameters of these kernels (a characteristic length of spatial dependency for each input variable) by maximum likelihood estimation using the BFGS optimization algorithm.

3.3 Putting it into practice

We performed 2548 simulations uniformly sampling the 5 dimensional input space of the release height, the wind module, the rain intensity and the two deposition velocity (their range of variation is given in table 1). The output dose being linear with the amplitude of the source term, we completed the simulation sample using two random amplitudes for each input vector, thus covering the whole 6 dimension input space with a total of 5096 points. 4096 of them are used to train the AAM, while the other 1000 were used to fit the model.

Because the dose values have important exponential variations with distance, we used the method on the logarithm of the dose. The AAM reduced the dimension of the results to nine coordinates, whereas the initial data dimension was 2196, corresponding to a grid mesh of size 36×61. Using fewer than nine coordinates resulted in larger errors, while higher-dimensional approximations increased computation times with only moderate improvements in results. Since the final goal of this parameterization is to focus on the zones where a dose threshold th is exceeded, we also truncated the logarithm of the doses: any values below $\log(th)/2$ were set to $\log(th)/2$. Thus, small dose variations do not disturb the parameterization by AAM.

Kriging is then used to create emulators. Once these emulators built, the emulator combined with dimension reduction can then be used to predict an output map for any new input vector (see figure 2). The AAM can finally associate to these 9 scalars a two dimensional map of inhalation dose.

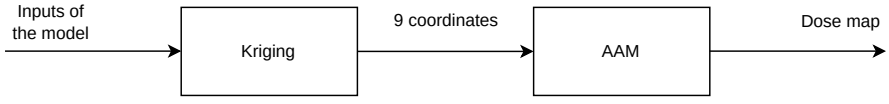

Figure 2. Dose map prediction process using emulation coupled with AAM.

4 Results

4.1 Validation

An additional simulation sample was built to test the reliability of the emulator. We drew $M = 1000$ random new points in our 6-dimensional input space and then run the computational model M times with input parameters corresponding to these draws. We obtained M output results that were compared with the maps reconstructed after dimension reduction with AAM (section 4.1.1) and with emulators predictions (section 4.1.2, then with the combination of the two methods (section 4.1.3).

https://doi.org/10.5194/egusphere-2024-3838
Preprint. Discussion started: 21 February 2025

4.1.1 Validation of the dimension reduction by AAM

We assessed the validity of the dimension reduction step by comparing the maps two by two for our test sample, as in figure 3, and by calculating the Figure of Merit in Space (FMS) of the dose criteria exceedance isolines for each of these maps. This score is calculated by dividing the area of the intersection of the two surfaces A and B by the area of the union of the two:

$$\text{FMS} = \frac{A \cap B}{A \cup B}$$

The FMS of two very similar surfaces approaches 1, while when two isolines have little surface in common it approaches 0.

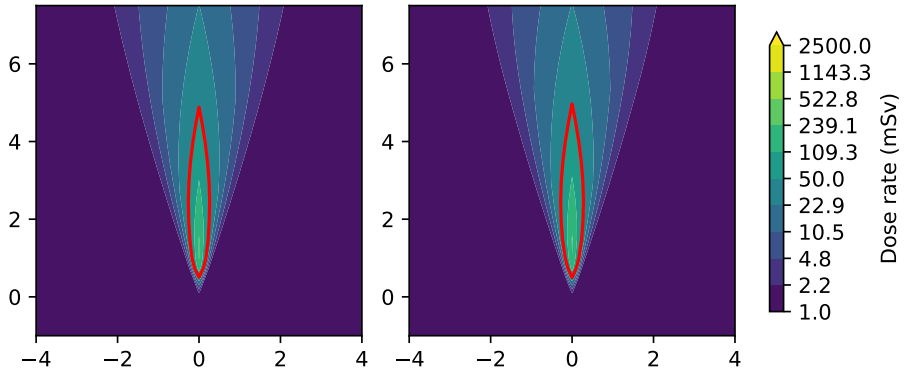

Figure 3. Inhalation dose map and 50 mSv guide-level exceedance isolines for a model output (left) and for the approximation of this output by AAM (right).

Figure 4 shows that the isolines exceeding 50 mSv are preserved with the AAM approximation. In 75.5% of the case, the FMS is above 0.8. In 11.7% of the case, the FMS cannot be calculated because there is no threshold exceedance. It means that the predicted isolines are very close to the one calculated by the model.

https://doi.org/10.5194/egusphere-2024-3838
Preprint. Discussion started: 21 February 2025

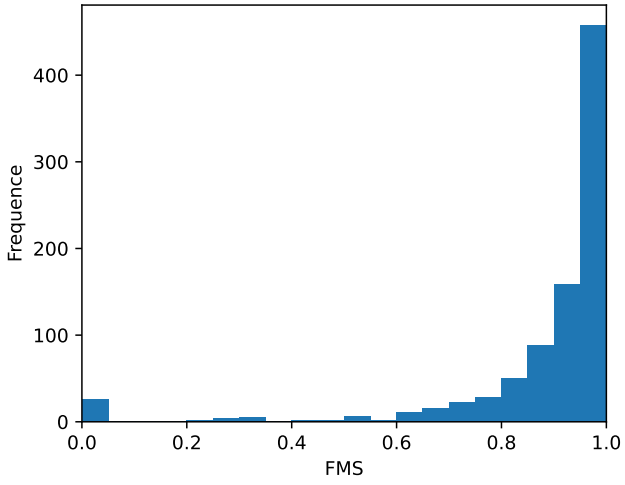

Figure 4. Histogram of the FMS that compares the threshold exceedance zones for the model outputs with AAM approximations.

4.1.2 Validation of the interpolation by Kriging

Figure 5 shows how well each scalar is predicted. The closer the set of points is to the line $y = x$, the better the prediction.

We quantified the prediction error with the Standardized Mean Squared Error (SMSE). For a set of N observed points $(x_i)_{i\in[1,N]}$ and a set $(\hat{x}_i)_{i\in[1,N]}$ of estimated points, the SMSE is defined as follows:

$$\text{SMSE} = \frac{\sum_{i=1}^{N}(x_i - \hat{x}_i)^2}{\sum_{i=1}^{N}(x_i - \bar{x})^2},$$

where $\bar{x}$ is the mean of $(x_i)_{i\in[1,N]}$.

Table 2. SMSE Calculated for Each Score

SMSE	Value
Score 01	9.939e-04
Score 02	6.482e-03
Score 03	1.466e-02
Score 04	7.065e-02
Score 05	1.228e-01
Score 06	6.076e-02
Score 07	1.604e-01
Score 08	5.114e-01
Score 09	1.001e+00

We can note in table 2 that the first three scalars are the best reconstructed. The last 2 scalars are the least well reconstructed.

https://doi.org/10.5194/egusphere-2024-3838
Preprint. Discussion started: 21 February 2025

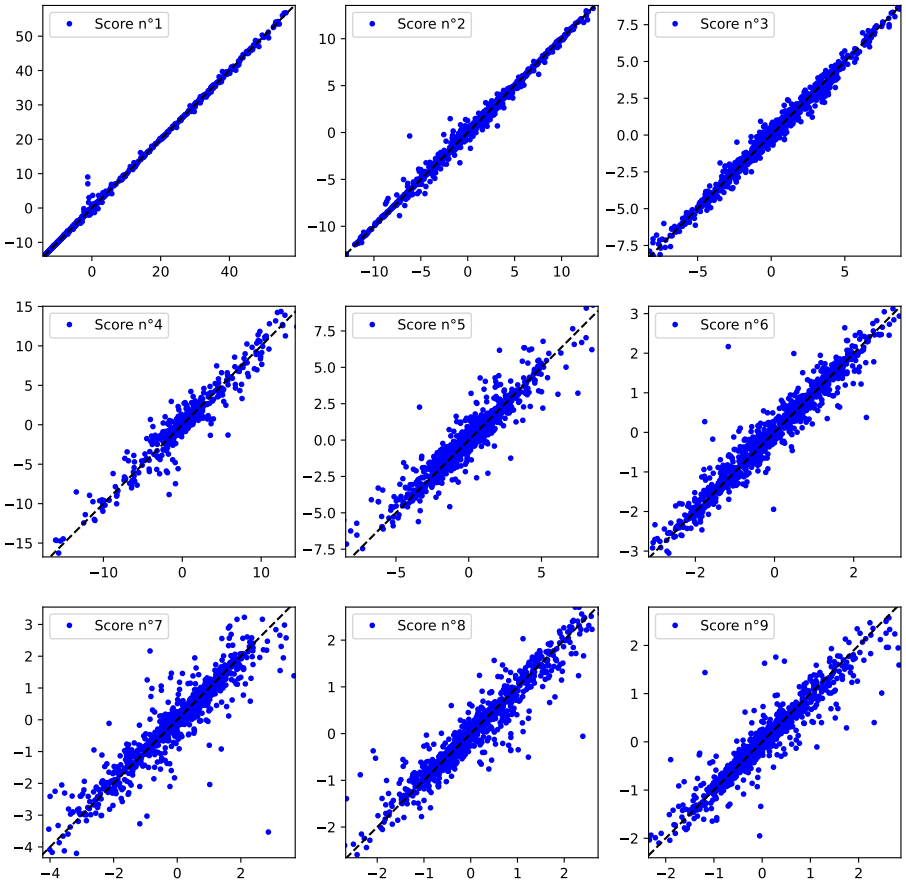

Figure 5. Comparison of the prediction of the emulator (in y-axis) with the target obtained by simulation (in x-axis). Each graph represent one coordinate of the AAM.

These results show that most scalars are well reconstructed by Kriging. The last scalars, even very poorly predicted, slightly improve the quality of the maps predicted by the method. This is why we decided to keep them.

4.1.3 Validation of the emulator that combines the two methods

With the AAM, this prediction of the 9 scalars can be transformed into a 2D dose map, which can be used to determine a threshold exceedance isoline. The succession of the two methods thus allows to convert the model inputs into a decision aiding map, defined by an isoline, to estimate whether or not a guide-level might be exceeded.

Comparisons between simulations and associated emulator predictions can be classified into four cases:

- Case 1: Dose maps that are well reconstructed by the method, as shown in figure 6 (a) and (b). The shape of the isoline is preserved, and its size is similar to that given by the simulation, resulting in a well-estimated maximum distance.

https://doi.org/10.5194/egusphere-2024-3838
Preprint. Discussion started: 21 February 2025

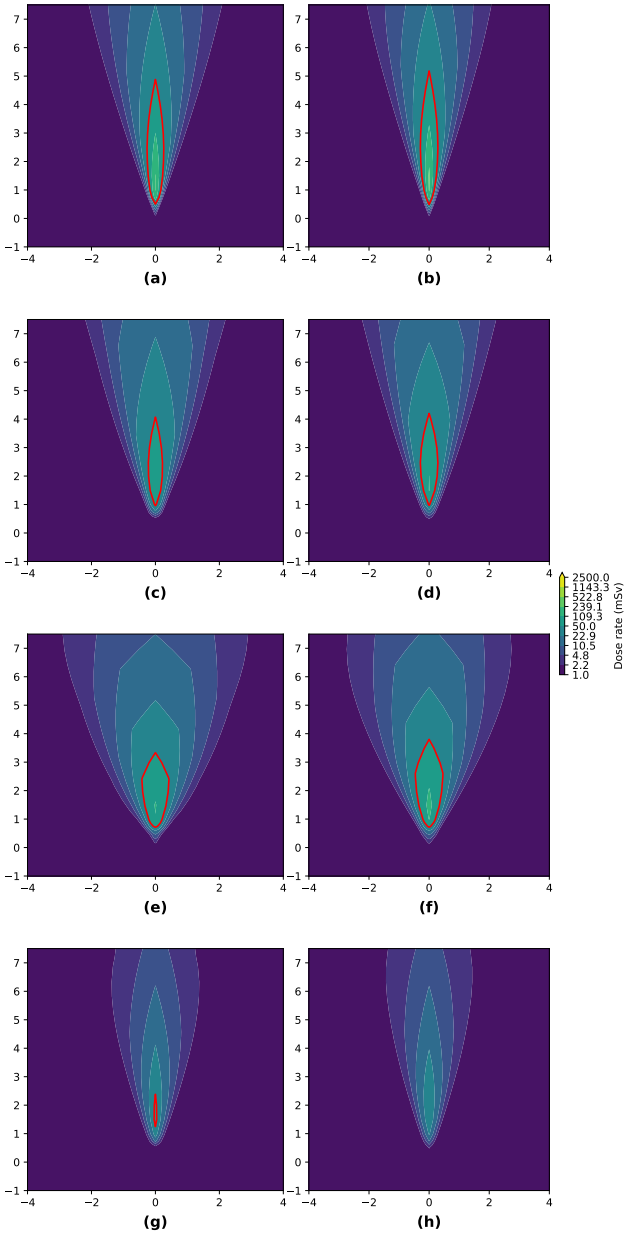

Figure 6. Examples of inhalation dose maps for simulated results by the original physical model (left) and emulator predicted results (right).

https://doi.org/10.5194/egusphere-2024-3838
Preprint. Discussion started: 21 February 2025

- Case 2: Dose maps that are well reconstructed, but the isolines can differ slightly in scale from what is expected, as illustrated in figure 6 (c) and (d).
- Case 3: Dose maps that are less well reconstructed, where the general shape of the isoline is not accurately reproduced. This typically occurs under low wind conditions, as shown in figure 6 (e) and (f).
- Case 4: Dose maps that approach the threshold value with little or no exceedance, but the predicted and simulated isolines may differ significantly. Figure 6 (g) and (h) illustrates this: although the two dose maps appear similar, a slight difference in intensity can cause a noticeable discrepancy in the exceedance isoline prediction.

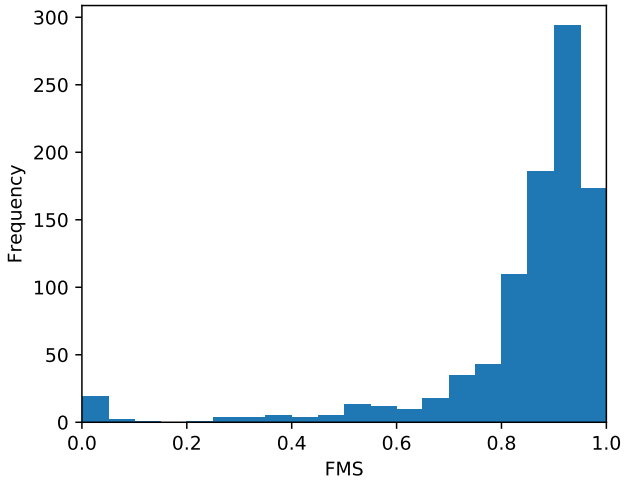

Figure 7. Histogram of the FMS that compares the threshold exceedance zones for the model outputs with the emulator outputs. 76.3 % of the FMS are between 0.8 and 1, which implies that the predicted results are very often similar to those obtained by simulation.

We evaluated the adequacy of the simulated and predicted surfaces by calculating the FMS of our test sample simulations. Figure 7 represents the histograms of the FMS. We can notice a slight degradation compared to Figure 4. However 70.9 % of the FMS are between 0.8 and 1, which implies that the predicted isolines are very often similar to those obtained by simulation (Case n°1 and n°2 described earlier). Also, 11.5 % of the FMS cannot be calculated, because both of the simulation and emulator detect no threshold exceedance. Those cases correspond also to a good prediction of the emulator. We note that 2.8 % of the FMS are equal to zero, which correspond to the problem of the non-reached threshold mentioned previously (Case n°3). The last 14.8 % intermediate FMS correspond to badly reconstructed isolines (Case n°4), for instance when the wind module is low, which does not necessarily mean that the surface error is large, because the FMS is a relative score. Excluding the cases where no threshold is exceeded, badly reconstructed areas amount to 17.6 %, which means that more than 80 % of the threshold exceedance areas are correctly forecast.

https://doi.org/10.5194/egusphere-2024-3838
Preprint. Discussion started: 21 February 2025

4.2 Comparison to other prediction methods

We benchmarked our new prediction method against two state of the art procedures:

- At the start of a crisis, a first estimate is derived from the ATS, yielding orders of magnitude and first results for distance and angular aperture of exceedance. Then simulations are performed with the pX model in order to predict a guide-level exceedance zone and estimate a maximum distance of threshold exceedance. An angular aperture is also estimated from pre-computed tables depending on wind, atmospheric stability, and meandering wind factor. This simulated maximum distance, associated with this angular aperture obtained without emulation, allows to deduce a portion of circle which corresponds to the zone for which decisions are recommended.

- In a previous study (Périllat et al., 2020), an emulator was created to directly predict, without using AAM, the maximum distance of the threshold exceedance given by the model, as well as the angular aperture of this zone. Kriging was used to estimate those two geometrical parameters from the original model pX.

These two methods will be referred to as the 'ATS estimator' and the 'Emulator of geometrical parameters' in the remainder of this paper.

https://doi.org/10.5194/egusphere-2024-3838
Preprint. Discussion started: 21 February 2025

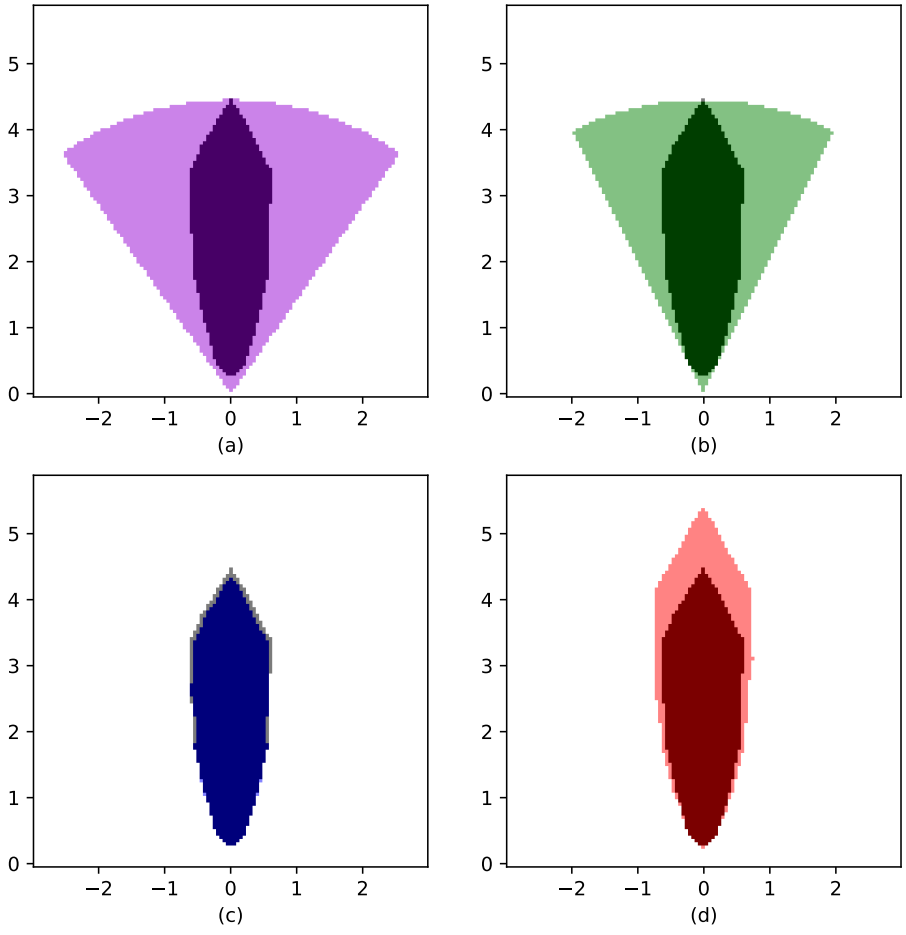

Figure 8. Guide-level exceedance zone, for one simulation of the test sample, obtained by the different estimation methods: the ATS estimator (a), the emulator of geometrical parameters (b), prediction by our emulator which coupled Kriging to AAM (c), prediction by the same emulator with a lower threshold (d). The zone of guide-level exceedance given by the Gaussian puff model pX is superimposed to each graph (darker color).

Figure 8 shows the comparison between the AAM-kriging emulator described in section 3 (Fig. 8(c)) and the two usual approaches (Fig. 8(a) and (b)). In addition, we tested a fourth method: the AAM-kriging emulator applied to a lower threshold exceedance than the actual guide-level value, to take a margin on the results obtained by the emulator (Fig. 8(d)). To achieve that, instead of creating an isoline at $\log(th)$ on our logarithmic dose, we created an isoline at $\log(th)/1.1$.

We compared the isolines of these different prediction methods to the one given by the Gaussian puff model for the 1000 simulations of our test sample. Four kinds of areas may be defined:

- True-Positives: areas where both the predictor and the model forecast a threshold exceedance.
- True-Negatives: areas where the predictor and the model do not forecast a threshold exceedance.

https://doi.org/10.5194/egusphere-2024-3838
Preprint. Discussion started: 21 February 2025

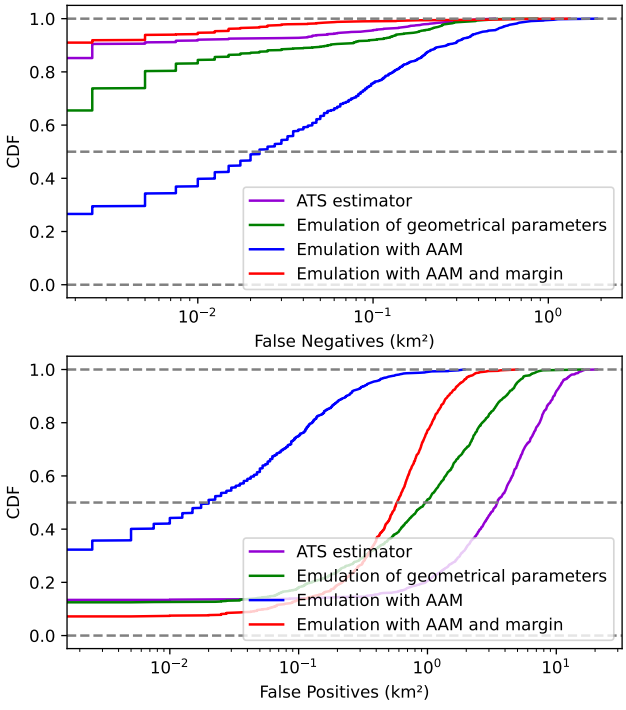

Figure 9. Cumulative distribution function of the probability to obtain surface of false-negative and false-positive (in km^2) for the different predictors. These functions where estimated with a sample test of 1000 simulations. The closer the curves are to the value 1, the lower the probability of obtaining false-negative (top) or false-positive (bottom).

- False-Positives: areas where the predictor predicts threshold exceedance, while the model forecasts the opposite.
- False-Negatives: areas where the predictor does not predict a threshold exceedance, while the model forecasts the opposite.

These surfaces allow us to evaluate the performance of each method. Each output pair (model, predictor) is characterized by a certain amount of true-positive, true-negative, false-positive and false-negative areas.

False-positive and false-negative are two kinds of errors that we seek to minimize, but the latter is the most critical as it would imply the underestimation of the population which could be exposed beyond the dose criteria.

Figure 9 and Table 3 show that the ATS estimator, used as a very first response, is the one that gives the most false-positives (10.665 km^2), with an extremely low number of false-negatives (0,030 km^2). This method was indeed designed to be conservative.

The emulator of geometrical parameters of the previous study have the advantage of decreasing the false-positives (3,846 km^2), but they increase the false-negative area (0,056 km^2), which are to be avoided as much as possible, as they are the most critical errors when considering population protection issues.

https://doi.org/10.5194/egusphere-2024-3838
Preprint. Discussion started: 21 February 2025

Estimator	Total surface (km^2)	
	False-Positive	False-Negative
ATS estimator	10.665	0,030
Emulator of geometrical parameters	3,846	0,056
AAM-kriging emulation	0,221	0,227
AAM-kriging emulation with margin	1,747	0,015

Table 3. Total surface in km^2 of false-positive and false-negative for the 1000 simulations of the sample text, for each method used to predict areas of dose threshold exceedance. The surface of the studied domain is 94,25 km^2.

The AAM-kriging emulation method gives few false-positives (0,221 km^2), and false-negatives (0,227 km^2), and in a similar quantity. Indeed, this method aims to get as close as possible to the isoline predicted by the original model. It therefore takes no margin and obtains small errors in either over- or under-estimation, demonstrating a fairly accurate prediction ability. The last method, designed by adding a margin thanks to a slightly lower threshold, slightly increases the false-positives (1,747 km^2), but drastically reduces the false-negatives (0,015 km^2). With this method, the number of false-negatives is as low as the quantity obtained by the ATS estimator, but with a number of false-positives more than eight times lower.

5 Application

AAM coupled with kriging allows the creation of emulators that can reproduce the model output in approximately 0.005 seconds, whereas the original dispersion model, pX, takes about 1 minute. This increased speed of calculation enables the use of the emulator in various applications where the use of the original model is not feasible.

This emulator can generate sample of thousands results in seconds, and then allow us to take the uncertainty into account in our study, by using probabilistic approaches, as it can be seen in figure 10 which shows an estimation of probability of threshold exceedance. We developed a graphical interface (see figure 11) enabling emergency responders to obtain the dose map immediately by modifying the input parameters. It can also be used as a training purpose, because it allows the user to see how the dose map evolves.

https://doi.org/10.5194/egusphere-2024-3838
Preprint. Discussion started: 21 February 2025

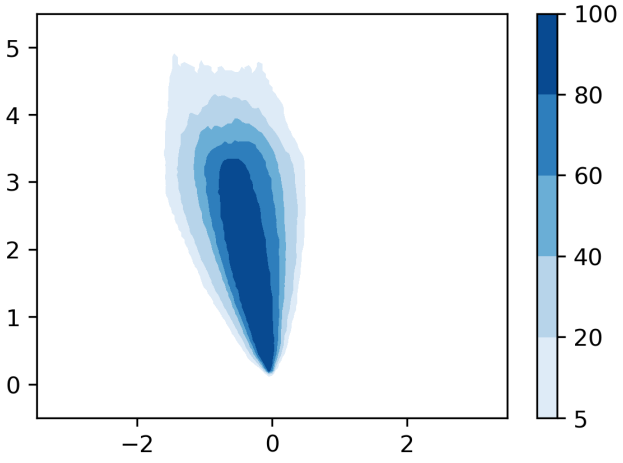

Figure 10. Example of a map which represent the estimation by the emulation with AAM of the probability of threshold exceedance after a nuclear accident.

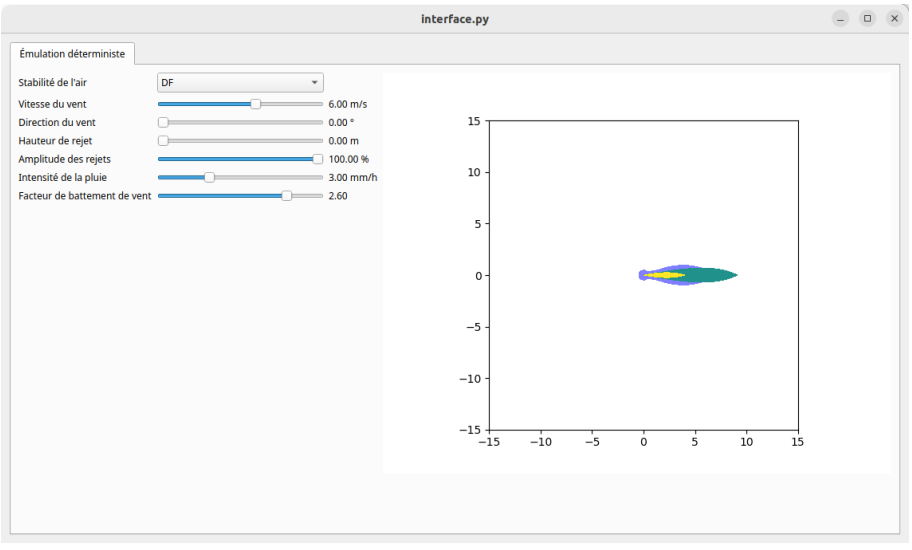

Figure 11. Example of a graphical interface created during the projet that enables users to directly observe how each input impacts the dose map.

6 Conclusion

AAM coupled with Kriging allow to create emulators which can reproduce the model output with a drastic reduction in computational time. The guide-level dose exceedance isoline obtained with the emulator is very close to the one obtained with the original model: the FMS between the two is under 0.8 in less than 17.6 % of our sample test. For an operational use, we

https://doi.org/10.5194/egusphere-2024-3838
Preprint. Discussion started: 21 February 2025

recommend to take a margin by reducing the threshold exceedance of the dose. It will slightly increase the false-positives, but significantly decrease the false-negatives.

We obtained very similar results with different guide-levels and with the Doury dispersion model in weak diffusion.

This method of creating emulator is currently in an operationalization phase, to reproduce it on several other source terms, to create a catalog of emulator which cover scenarios among the ATS of ASNR.

This is the first time the AAM are used on a real and operational application. This study advances the state of the art in atmospheric dispersion by creating a new way to parameterize and predict quantity maps, which can be used in an operational context with probabilistic approaches where hundreds of results must be obtained.

The main limitation of our approach is that in some rare cases, mainly when the wind module is low, the emulator's ability to reconstruct the model's predicted map is lower. However, these cases are also badly forecast by the physical dispersion model itself, and the error of the emulator would not necessarily exceed that of the pX model, were they compared to environmental observations. We think that these results would be improved by modifying the AAM construction method, which at some point in its process uses a Euclidean distance to compare maps. However, some mathematical distances, such as the Wasserstein distance (Kolouri et al., 2017) for example, could be more suitable for comparing 2D dose maps within them. The AAM method could then benefit from a modification to use other distances in its algorithm to go one step further in improving the application cases.

Code and data availability. The code used for generating and analyzing the simulation data is publicly available on GitLab at https://gitlab.com/perillat/emulation_aam. The simulation data is hosted on Zenodo with the DOI: 10.5281/zenodo.14747261.

Competing interests. The authors declare that they have no conflict of interest.

Author contributions. R.P. developed the software, analyzed the data, contributed to the study design and methodology, and wrote the manuscript with input from all co-authors. S.G. and I.K. contributed to the study design and methodology. I.K. supervised the research.

https://doi.org/10.5194/egusphere-2024-3838
Preprint. Discussion started: 21 February 2025

References

Burgin, L., Ekström, M., and Dessai, S.: Combining dispersion modelling with synoptic patterns to understand the wind-borne transport into the UK of the bluetongue disease vector, International Journal of Biometeorology, 61, 1233–1245, https://doi.org/10.1007/s00484-016-1301-1, 2017.

Chilès, J.-P. and Delfiner, P.: Geostatistics, modeling spatial uncertainty, John Wiley & sons, 1999.

de l'intérieur, M.: Déclinaison du plan national de réponse à un accident nucléaire ou radiologique majeur, https://mobile.interieur.gouv.fr/content/download/122901/985795/file/Guide_S4_tome_1_d/%C3/%A9clinaison_PNRANRM.pdf.

El-Ouartassy, Y., Korsakissok, I., Plu, M., Connan, O., Descamps, L., and Raynaud, L.: Combining short-range dispersion simulations with fine-scale meteorological ensembles: probabilistic indicators and evaluation during a Kr-85 field campaign, Atmospheric Chemistry and Physics, 22, 15 793–15 816, https://doi.org/10.5194/acp-22-15793-2022, 2022.

Fukunaga, K. and Olsen, D. R.: An Algorithm for Finding Intrinsic Dimensionality of Data, IEEE Transactions on Computers, C-20, 176–183, https://doi.org/10.1109/t-c.1971.223208, 1971.

Girard, S.: A nonlinear PCA based on manifold approximation, Computational Statistics, 15, 145–167, https://hal.inria.fr/hal-00724764, 2000.

Girard, S. and Iovleff, S.: Auto-associative models, nonlinear Principal component analysis, manifolds and projection pursuit, in: Principal Manifolds for Data Visualisation and Dimension Reduction, edited by Alexander N. Gorban and Balázs Kégl and Donald C. Wunsch and and Andrei Y. Zinovyev, vol. 58 of *Lecture Notes in Computational Science and Engineering*, pp. 202–218, Springer-Verlag, https://doi.org/10.1007/978-3-540-73750-6_8, 2008.

Girard, S., Korsakissok, I., and Mallet, V.: Screening sensitivity analysis of a radionuclides atmospheric dispersion model applied to the Fukushima disaster, Atmospheric Environment, 95, 490–500, https://doi.org/http://dx.doi.org/10.1016/j.atmosenv.2014.07.010, 2014.

Girard, S., Mallet, V., Korsakissok, I., and Mathieu, A.: Emulation and Sobol' sensitivity analysis of an atmospheric dispersion model applied to the Fukushima nuclear accident, Journal of Geophysical Research: Atmospheres, https://doi.org/10.1002/2015jd023993, 2016.

Girard, S., Armand, P., Duchenne, C., and Yalamas, T.: Stochastic perturbations and dimension reduction for modelling uncertainty of atmospheric dispersion simulations, Atmospheric Environment, p. 117313, https://doi.org/10.1016/j.atmosenv.2020.117313, 2020.

Jolliffe, I. T.: Principal Component Analysis, Springer, 2ème edn., 2002.

Jolliffe, I. T. and Cadima, J.: Principal component analysis: a review and recent developments, Philosophical Transactions of the Royal Society A: Mathematical, Physical and Engineering Sciences, 374, 20150 202, https://doi.org/10.1098/rsta.2015.0202, 2016.

Kolouri, S., Park, S. R., Thorpe, M., Slepcev, D., and Rohde, G. K.: Optimal Mass Transport: Signal processing and machine-learning applications, IEEE Signal Processing Magazine, 34, 43–59, https://doi.org/10.1109/MSP.2017.2695801, 2017.

Korsakissok, I., Mathieu, A., and Didier, D.: Atmospheric dispersion and ground deposition induced by the Fukushima Nuclear Power Plant accident: A local-scale simulation and sensitivity study, Atmospheric Environment, 70, 267–279, https://doi.org/https://doi.org/10.1016/j.atmosenv.2013.01.002, 2013.

Le, N. B. T., Mallet, V., Korsakissok, I., Mathieu, A., Perillat, R., and Didier, D.: Metamodeling and optimization of probabilistic scores for long-range atmospheric dispersion applied to the Fukushima nuclear disaster, in: EGU General Assembly Conference Abstracts, vol. 20, p. 17209, 2018.

https://doi.org/10.5194/egusphere-2024-3838
Preprint. Discussion started: 21 February 2025

LE, N. B. T., Korsakissok, I., Mallet, V., Périllat, R., and Mathieu, A.: Uncertainty study on atmospheric dispersion simulations using meteorological ensembles with a Monte Carlo approach, applied to the Fukushima nuclear accident, Atmospheric Environment: X, 10, 100 112, https://doi.org/https://doi.org/10.1016/j.aeaoa.2021.100112, 2021.

Leadbetter, S.J., Andronopoulos, S., Bedwell, P., Chevalier-Jabet, K., Geertsema, G., Gering, F., Hamburger, T., Jones, A.R., Klein, H., Korsakissok, I., Mathieu, A., Pázmándi, T., Périllat, R., Rudas, Cs., Sogachev, A., Szántó, P., Tomas, J.M., Twenhöfel, C., de Vries, H., and Wellings, J.: Ranking uncertainties in atmospheric dispersion modelling following the accidental release of radioactive material, Radioprotection, 55, S51–S55, https://doi.org/10.1051/radiopro/2020012, 2020.

Lumet, E., Rochoux, M. C., Jaravel, T., and Lacroix, S.: Uncertainty-aware surrogate modeling for urban air pollutant dispersion prediction, Building and Environment, 267, 112 287, https://doi.org/https://doi.org/10.1016/j.buildenv.2024.112287, 2025.

Mallet, V., Tilloy, A., Poulet, D., Girard, S., and Brocheton, F.: Meta-modeling of ADMS-Urban by dimension reduction and emulation, Atmospheric Environment, 184, 37–46, https://doi.org/10.1016/j.atmosenv.2018.04.009, 2018.

Milnor, J. W.: Topology from the differentiable viewpoint, Princeton university press, 1997.

Nomura, S., Gilmour, S., Tsubokura, M., Yoneoka, D., Sugimoto, A., Oikawa, T., Kami, M., and Shibuya, K.: Mortality Risk amongst Nursing Home Residents Evacuated after the Fukushima Nuclear Accident: A Retrospective Cohort Study, PLOS ONE, 8, 1–9, https://doi.org/10.1371/journal.pone.0060192, 2013.

Nomura, S., Blangiardo, M., Tsubokura, M., Ozaki, M., and Hodgson, S.: Postnuclear disaster evacuation and chronic health in adults in Fukushima, Japan: a long-term retrospective analysis, BMJ Open, 6, 1–9, https://doi.org/10.1136/bmjopen-2015-010080, 2016.

Périllat, R., Korsakissok, I., Girard, S., and Quentric, E.: Emulators for the rapid prediction of consequences in case of nuclear hazards, in: 20th International Conference on Harmonisation within Atmospheric Dispersion Modelling for Regulatory Purposes, HARMO20, Tartu, Estonia, 2020.

Roustant, O., Ginsbourger, D., and Deville, Y.: DiceKriging, DiceOptim: two R packages for the analysis of computer experiments by kriging-based metamodeling and optimization, Journal of Statistical Software, 51, 1–55, 2012.

Swallow, B., Rigby, M., Rougier, J. C., Manning, A. J., Lunt, M., and O'Doherty, S.: Parametric uncertainty in complex environmental models: a cheap emulation approach for models with high-dimensional output, 2017.

Tombette, M., Quentric, E., Quélo, D., Benoit, J.-P., Mathieu, A., Korsakissok, I., and Didier, D.: C3X: A software platform for assessing the consequences of an accidental release of radioactivity into the atmosphere, 2014.